Stabilizing Quasi-Time-Optimal Nonlinear Model Predictive Control with Variable Discretization

Christoph Rösmann, Artemi Makarow, and Torsten Bertram

Abstract—This paper deals with the development and analysis of novel time-optimal point-to-point model predictive control concepts for nonlinear systems. Recent approaches in the literature apply a time transformation, however, which do not maintain recursive feasibility for piecewise constant control parameterization. The key idea in this paper is to introduce uniform grids with variable discretization. A shrinking-horizon grid adaptation scheme ensures convergence to a specific region around the target state and recursive feasibility. The size of the region is configurable by design parameters. This facilitates the systematic dual-mode design for quasi-time-optimal control to restore asymptotic stability and establish a smooth stabilization. Two nonlinear program formulations with different sparsity patterns are introduced to realize and implement the underlying optimal control problem. For a class of numerical integration schemes, even nominal asymptotic stability and true time-optimality are achieved without dual-mode. A comparative analysis as well as experimental results demonstrate the effectiveness of the proposed techniques.

Index Terms—Predictive control, Minimum-time control, Time-optimal control, Direct transcription, Variable discretization, Hypergraph, Dual-mode

I. Introduction

Minimizing time plays a vital role in increasing the productivity of automation solutions in a variety of industries. To give a few examples, in the field of warehouse robotics, mobile robots are expected to navigate as fast as possible while avoiding obstacles. The productivity in the area of automated assembly at automobile manufacturers correlates strongly with the execution speed of their robotic manipulators. Also, racing is dedicated to minimizing lap times as a central objective.

A comprehensive and generic framework to explicitly account for performance criteria during feedback control is nonlinear model predictive control (MPC) [1], [2]. Researches in the context of MPC mainly consider quadratic cost terms as performance criteria, in particular, the minimization of the state error and control effort. In the recent years, also the study of economic MPC schemes with arbitrary performance criteria has received major attention. However, the theoretical foundation and findings do not necessarily include minimum-time formulations as these usually require non-fixed final times in the prediction horizon. The literature mentions dedicated time-optimal MPC realizations rarely. Nevertheless, some contributions and applications rely on a time transformation from feedforward optimal control [3], [4]. Hereby, the variable grid is mapped on to a fixed grid in a new time scale and

The authors are with the Institute of Control Theory and Systems Engineering, TU Dortmund University, D-44227, Germany, (e-mail: christoph.roesmann@tu-dortmund.de).

accordingly the system dynamics equation is scaled by additional optimization parameters. Stability results for controllers considering the time transformation with simple state feedback are still intractable, especially due to the control parameterization applied in direct optimal control and MPC, and are hence not yet available in the literature (see also [5]). Zhao et al. provide a time-optimal MPC scheme for the control of a spherical robot based on the time transformation [6]. A hybrid cost function that also considers quadratic form cost achieves stabilization. The transformed time is bounded from below close to the target state such that only the quadratic form cost becomes active. However, the approach does not guarantee recursive feasibility. Verschueren et al. compute time-optimal motions along a Cartesian path for robotic manipulators [7]. Time transformation is applied to the underlying time-optimal control problem to map states and controls onto a fixed integration grid. In applications such as race car automatic control, tailored MPC methods minimize the lap time [8]–[11].

A nonlinear MPC method for time-optimal point-to-point transitions which does not rely on time transformation is presented in [12], [13]. The method called TOMPC minimizes the settling time, i.e. horizon length N, in a two-layer optimization routine. The outer loop incrementally decreases N until the inner loop nonlinear program with a standard quadratic form cost fails to generate a feasible solution for the allocated time horizon. Since the cost function minimizes the distance of discrete states to the final state, the solution with the shortest feasible horizon is quasi time-optimal. Due to the lower bound on the time horizon, the algorithm behaves like a conventional MPC in the vicinity of the final state and therefore guarantees asymptotic stability. The computation time strongly depends on the initial estimate of the settling time, as it determines the number of iterations in the outer loop time horizon reduction. Properties on time-optimal MPC for discrete-time systems in general are discussed in [14]. An alternative approach that follows a reference path in minimum time is presented in [15]. Time-optimality is nearly achieved in case of long time horizons. A time-optimal approach for linear systems is presented in [16].

An approach that considers ℓ_1-norm cost functions for linear systems is described in [17]. For general nonlinear systems, Verschueren et al. proposes a stabilizing time-optimal MPC approach based on a weighted ℓ_1-norm cost [5]. The approach considers discrete-time respectively sampled-data models and guides the system towards a target state in minimum time and stabilizes it there. It is required that the horizon length N is sufficiently large such that the target state is reachable within

N time steps. The single-stage optimization as well as milder assumptions on N are superior in comparison to TOMPC. Since the ℓ_1-norm is non-smooth, it is replaced by a smooth representation in every practical implementation. It consists of additional slack variables which might increase computation times significantly for larger problems. In addition, a weighting parameter must be chosen properly to ensure time-optimality while maintaining numerical well-conditioning of the underlying optimization problem.

Previous work proposes time-optimal point-to-point MPC formulations based on direct transcription and variable discretization [18], [19]. A dedicated grid adaptation scheme adjusts the temporal resolution with respect to a predefined sample time during runtime. However, the presented work does not take stability and recursive feasibility maintenance and guarantees into account. To this end, these important challenges are addressed in this paper and the novel contributions are as follows: Time-optimal MPC with variable discretization is formulated based on sampled-data systems with piecewise constant control parameterization, instead of relying on direct transcription initially [20]. A shrinking horizon grid adaptation scheme enables the derivation of convergence and recursive feasibility results. The size of the target region which is guaranteed to be reached is adjusted by design of the controller, e.g. by choosing a proper grid size. In addition, the derivation of these results include lower bounds on the temporal resolution and grid size, which are often indispensable in practice. The theoretical results either allow *a true time-optimal point-to-point transition* to adhere to predefined tolerances or enable *a systematic quasi-time-optimal dual-mode controller design* which restores true asymptotic stability. Finally, two nonlinear program formulations with different sparsity patterns are presented that mimic the optimal control problem. Depending on the underlying numerical integration scheme and stricter conditions, even asymptotic stability results are derived for the nominal system without dual-mode realization.

The outline of this paper is as follows: Section II introduces some preliminaries and a formal description of the MPC realization. Section III discusses stability and recursive feasibility issues, proposes a grid adaptation scheme and presents convergence results. Details on the practical realization are provided in Section IV. Quasi-time optimal stabilizing control based on dual-mode is described in Section V. Section VI provides a numerical example and compares the proposed techniques with the state of the art. A demonstration on a real system is provided in Section VII, and finally Section VIII concludes the work.

II. Preliminaries and Problem Setup

A. Notation

Let $\mathbb{N}_0$ denote the set of non-negative integers and $\mathbb{R}_0^+$ the set of non-negative real numbers. Furthermore, $\emptyset$ represents an empty set. Let $\mathrm{D}_u f(\bar{u})$ denote the Jacobian of f w.r.t. u and evaluated at $\bar{u}$. The set of Lebesgue integrable mappings from interval $I \subseteq \mathbb{R}$ to $\mathbb{R}^q$ is denoted by $L^\infty(I, \mathbb{R}^q)$.

B. Dynamic System

We consider continuous-time, nonlinear, time-invariant systems with state trajectory $x : \mathbb{R} \mapsto \mathcal{X}$ and control trajectory $u : \mathbb{R} \mapsto \mathcal{U}$:

$$\dot{x}(t) = f\big(x(t), u(t)\big). \tag{1}$$

Throughout this paper, the state space $\mathcal{X}$ and control space $\mathcal{U}$ are defined as $\mathcal{X} := \mathbb{R}^p$ and $\mathcal{U} := \mathbb{R}^q$ with state vector dimension $p \in \mathbb{N}$ and control vector dimension $q \in \mathbb{N}$ respectively. Function $f : \mathcal{X} \times \mathcal{U} \mapsto \mathcal{X}$ defines a nonlinear mapping of the state and control trajectory, $x(t)$ and $u(t)$ respectively, to the state velocity $\dot{x}(t)$ embedded in $\mathcal{X}$. System (1) is further subject to state and input constraint sets, i.e. $x(t) \in \mathbb{X} \subseteq \mathcal{X}$ and $u(t) \in \mathbb{U} \subset \mathcal{U}$, respectively. The solution to (1) contained in an open time interval $I \subseteq \mathbb{R}$ with initial value $x(t_\mathrm{s}) = x_\mathrm{s}$, $t_\mathrm{s} \in I$, $x_\mathrm{s} \in \mathcal{X}$ and $t \in I$ is defined by

$$\varphi\big(t, x_\mathrm{s}, u(t)\big) = x_\mathrm{s} + \int_{t_\mathrm{s}=0}^{t} f\big(x(\tau), u(\tau)\big) \mathrm{d}\tau. \tag{2}$$

Without loss of generality, initial time t_s is fixed to $t_\mathrm{s} = 0$ as (1) is time-invariant. Carathéodory's existence theorem addresses conditions for the existence and uniqueness of the solution. In the following, we assume that the vector field f is continuous and Lipschitz in its first argument. Furthermore, the control $u(t)$ is supposed to be locally Lebesgue integrable for $t \in I$, i.e. $u \in L^\infty(I, \mathcal{U})$.

C. Optimal Control Problem

In MPC, system (1) is considered as dynamic model for the underlying optimal control problem to predict the future evolution. As in the majority of MPC realizations, the control trajectory is parameterized as piecewise constant which also reflects the discrete-time nature of the inherent sampled control law. To this end, consider the following grid: $0 = t_0 \leq t_1 \leq \ldots \leq t_k \leq \ldots \leq t_N = t_\mathrm{f}$ with $t_k, t_\mathrm{f} \in I$, $k = 0, 1, \ldots, N$ and $N \in \mathbb{N}$. Condition $t_{k+1} - t_k = \Delta t$ for $k = 0, 1, \ldots, N-1$ enforces uniformity with grid partition length $\Delta t \in \mathbb{R}_0^+$ and hence $t_k = k\Delta t$ refers to individual grid points. Restricting the control trajectory $u(t)$ to constant values $u_k \in \mathcal{U}$ on each grid partition results in the following control function space:

$$\begin{aligned}
\mathcal{U}^N(t_\mathrm{f}) :=& \{u \in L^\infty([0, t_\mathrm{f}], \mathcal{U}) \mid \exists u_0, u_1, \ldots, u_{N-1} \in \mathcal{U}, \\
& u(t) := u_k \text{ for } t \in [t_k, t_{k+1}) \text{ with } t_k = kt_\mathrm{f}/N, \\
& k = 0, 1, \ldots, N-1\}.
\end{aligned} \tag{3}$$

The control task considered in this paper comprises the motion from an initial state x_s to a target set $\mathbb{X}_\mathrm{f} \subseteq \mathbb{X}$ in minimum time. In fact, we focus primarily on point-to-point motions such that $\mathbb{X}_\mathrm{f}$ is given by $\mathbb{X}_\mathrm{f} := \{x_\mathrm{f}\}$ with terminal state $x_\mathrm{f} \in \mathbb{X}$. A control trajectory $u \in \mathcal{U}^N(t_\mathrm{f})$ and the corresponding state trajectory $\varphi\big(t, x_\mathrm{s}, u(t)\big)$ are called *admissible for x_s up to time t_f in N steps* if $u(t) \in \mathbb{U}$, $\varphi\big(t, x_\mathrm{s}, u(t)\big) \in \mathbb{X}$ for $t \in [0, t_\mathrm{f})$ and $\varphi\big(t_\mathrm{f}, x_\mathrm{s}, u(t)\big) \in \mathbb{X}_\mathrm{f}$ hold. Accordingly, the function space of all admissible control trajectories is denoted by:

$$\begin{aligned}
\mathscr{U}^N(x_\mathrm{s}, t_\mathrm{f}) :=& \{u \in \mathcal{U}^N(t_\mathrm{f}) \mid u(t) \in \mathbb{U}, \varphi\big(t_\mathrm{f}, x_\mathrm{s}, u(t)\big) \in \mathbb{X}_\mathrm{f} \\
& \text{for } t \in [0, t_\mathrm{f}], \varphi\big(kt_\mathrm{f}/N, x_\mathrm{s}, u(t)\big) \in \mathbb{X} \text{ for} \\
& t \in [0, (k+1)t_\mathrm{f}/N) \text{ and } k = 0, 1, \ldots, N-1\}.
\end{aligned} \tag{4}$$

Remark 1: Note, that the admissibility definition (4) considers state constraints only at grid points, which is common in sampled-data MPC. However, the results in Section III also apply to a definition in which $\varphi\big(t, x_s, u(t)\big) \in \mathbb{X}$ holds for $t \in [0, t_f)$.

The optimal control problem of searching for the minimum transition time and corresponding control trajectory is now expressed compactly in mathematical form:

$$t_f^*(x_s, N) = \min_{u \in \mathscr{U}^N(x_s, t_f), t_f} t_f \quad \text{s.t.} \quad N\Delta t_{\min} \leq t_f \leq N\Delta t_{\max}. \tag{5}$$

Hereby, $t_f^*(x_s, N)$ denotes the minimum transition time and emphasizes its relation to initial state x_s and grid resolution N. Bounds $\Delta t_{\min}, \Delta t_{\max} \in \mathbb{R}_0^+$ with $\Delta t_{\min} \leq \Delta t_{\max}$ are of a technical nature and their purpose is described later. We denote the resulting optimal control trajectory by $u^*(t, x_s, N)$ and the optimal grid partition length by $\Delta t^*(x_s, N) = t_f^*(x_s, N)/N$. Note that the grid is time-variable similar to [18]. The optimal control problem (5) is referred to as *feasible* if the resulting optimal control and state trajectories are admissible from x_s up to time $t_f^*(x_s, N)$ in N steps. Closely related to feasibility is the notion of viability which implies feasibility. A specialized definition to account for the variable final time, terminal condition and the previously defined control parameterization is given as follows: The tuple $(\mathbb{X}, \mathbb{X}_f)$ is called *viable for grid size N* if for each $x_s \in \mathbb{X}$ there exists $t_f \geq 0$ such that $\mathscr{U}^N(x_s, t_f) \neq \emptyset$ holds.

D. Closed-Loop Control

In the following, the previously defined optimal control problem (5) is integrated with state feedback. Since (5) can only be solved at discrete time instances, the sampled feedback control law is defined according to the grid $t_{\mu,0} < t_{\mu,1} < \ldots < t_{\mu,n} < \ldots < \infty$ with $n \in \mathbb{N}_0$ and $t_{\mu,n} \in \mathbb{R}_0^+$. Hereby, subscript μ indicates that the context belongs to the evolution of the closed-loop system. To account for the time-variable grid, the interval length $[t_{\mu,n}, t_{\mu,n+1}]$ at time instance n is inherited from the first interval of the corresponding prediction (5). In particular, the implicit control law $\mu_N : \mathcal{X} \mapsto \mathcal{U}$ for $t_\mu \in [t_{\mu,n}, t_{\mu,n} + \Delta t_{\mu,n})$ with $\Delta t_{\mu,n} := \Delta t^*\big(x_\mu(t_{\mu,n}), N\big)$ is defined by:

$$\mu_N\big(x_\mu(t_\mu)\big) := u^*\big(0, x_\mu(t_{\mu,n}), N\big). \tag{6}$$

Hereby, $x_\mu : \mathbb{R}_0^+ \mapsto \mathcal{X}$ denotes the closed-loop state trajectory which is either directly measured or obtained by a state observer.

Considering the plant dynamics (1) and control law (6), the resulting closed-loop system with initial state $x_s \in \mathcal{X}$ at time $t_{\mu,0}$ is defined by:

$$\dot{x}_\mu(t_\mu) = f\Big(x_\mu(t_\mu), \mu_N\big(x_\mu(t_\mu)\big)\Big), \quad x_\mu(t_{\mu,0}) = x_s. \tag{7}$$

According to (2), the corresponding closed-loop state evolution is obtained by:

$$x_\mu(t_\mu) := \varphi_\mu\big(t_\mu, t_{\mu,0}, x_s\big) := \varphi\Big(t_\mu - t_{\mu,0}, x_s, \mu_N\big(x_\mu(t_\mu)\big)\Big). \tag{8}$$
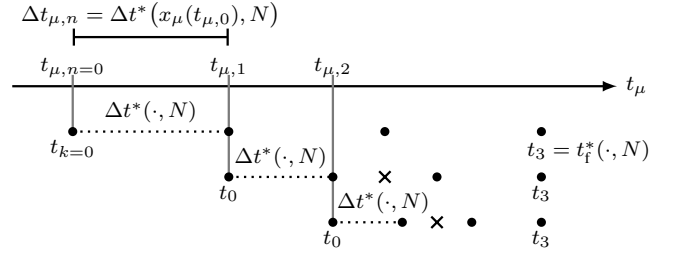

Fig. 1: Illustration of the closed-loop grid with constant size N. The dots correspond to the discretization grid of the prediction at closed-loop sampling times $t_{\mu,n}$. Crosses indicate a potential lack of recursive feasibility.

III. STABILITY ANALYSIS AND CONTROLLER DESIGN

This section analyzes the stability properties of closed-loop system (7) and proposes an additional grid adaptation scheme to improve the closed-loop performance. Whereas standard MPC formulations with terminal equality condition $\mathbb{X}_f := \{x_f\}$ usually enforce asymptotic stability [1], this observation does not apply to time-variable grids and optimal control problem (5) in particular. The following stability results explicitly account for these types of grids and are based on the principle of optimality [21]. We first define the a controllability region specialized for this setup:

Definition 1 (Controllability Region): The set which contains all states $\tilde{x} \in \mathbb{X}$ from that the terminal set $\mathbb{X}_f$ is reachable within N steps and at least a transition time $t_c \in \mathbb{R}_0^+$ is defined by:

$$P_c(N, t_c) := \big\{\tilde{x} \in \mathbb{X} \mid \mathscr{U}^N(\tilde{x}, t) \neq \emptyset, 0 \leq t \leq t_c\big\}. \tag{9}$$

Note, this set relates to viability up to time t_c. It is further equivalent to the reachable set from $\mathbb{X}_f$ in time t_c and the backward respectively reverse-time system $\dot{x}(t) = -f\big(x(t), u(t)\big)$ [22]. Determining $P_c(N, t_c)$ analytically is usually difficult and common numerical methods to obtain reachable or controllable sets can be applied [22]. For instance simulations can be performed for low-dimensional systems, or an auxiliary optimal control problem can be solved which maximizes the target set (reachable set) w.r.t. the backward dynamics [23].

A. Stability and Recursive Feasibility Issues

Forward invariance is often ensured by maintaining recursive feasibility during closed-loop transition. As a requirement, the first optimal control problem must be feasible which is, e.g., addressed by the viability assumption. However, the control parameterization in optimal control problem (5) invalidates recursive feasibility guarantees for closed-loop system (7). Since the grid is uniform with size N and the final state is subject to terminal conditions, the time interval decreases as the closed-loop system evolves, i.e. $\Delta t^*\big(x_\mu(t_{\mu,n}), N\big) \to \Delta t_{\min}$ for $n \to \infty$ (see Figure 1). Correspondingly, grid points t_k of the very first optimal control problem do not coincide with the closed-loop sampling instances $t_{\mu,n}$. Hence, Bellman's principle of optimality does not hold anymore. The prediction at $t_{\mu,1}$ cannot realize a switch in control at t_2 of the previous solution (marked by a cross symbol).
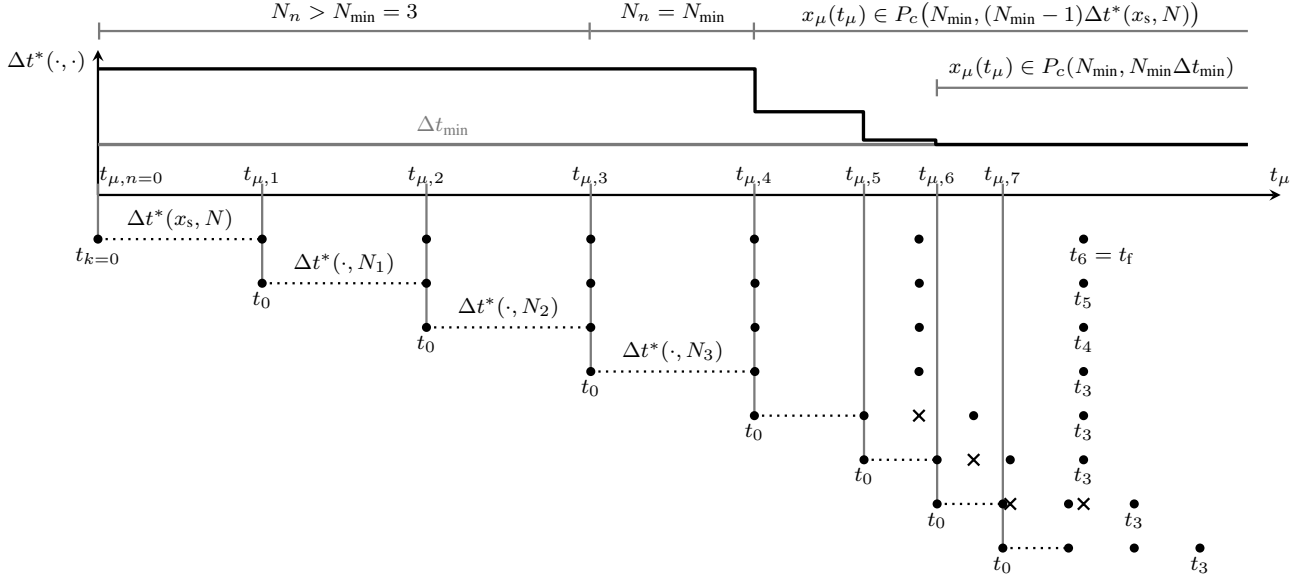
Fig. 2: Illustration of the different stages during closed-loop control. The points correspond to the discretization grid of the prediction (horizon) at closed-loop sampling times $t_{\mu,n}$. Crosses indicate a potential lack of recursive feasibility for states within the region $P_c\big(N_{\min}, (N_{\min}-1)\Delta t^*(x_s, N)\big)$. As soon as $\Delta t^* = \Delta t_{\min}$ is reached, that is for $x_\mu(t_\mu) \in P_c(N_{\min}, N_{\min}\Delta t_{\min})$, the cost no longer decreases and thus the temporal grid/horizon length is fixed and becomes receding. However, time-optimality and proper stabilization at x_f is no longer guaranteed.

In addition, $\Delta t^*\big(x_\mu(t_{\mu,n}), N\big) \to 0$ for $n \to \infty$ and $\Delta t_{\min} = 0$ implies the following drawbacks: First, the terminal set/state $\mathbb{X}_f$ cannot be reached in finite time. Secondly and more technically, small time intervals result in ill-conditioned optimization problems and thus affect convergence.

Consider the case $x_\mu(t_\mu) \in \mathbb{X}_f$. For $\Delta t_{\min} = 0$, the optimal time interval is $\Delta t^*(x_\mu(t_\mu), N) = 0$ and hence evaluating control law (6) reveals the following difficulties: Neither an infinite sampling rate can be realized in practice, nor does the imminent control action $u^*(0, x_\mu(t_\mu), N)$ ensures keeping the system in $\mathbb{X}_f$. As $t_f = 0$ holds, any admissible control satisfies $\varphi\big(0, x_f, u(t)\big)$ in (2) and (5) and thus forward invariance of $\mathbb{X}_f$ cannot be guaranteed in general.

B. Grid Adaption and Closed-Loop Convergence

This section proposes a modification that accounts for the previously discussed issues. The lack of recursive feasibility and finite-time convergence are addressed by reducing the grid size N while the closed-loop system evolves. Let $N_n \in \mathbb{N}$ denote the grid size at time instance $t_{\mu,n}$ with $n \in \mathbb{N}_0$. The initial grid size $N_0 := N$ is set to a user-defined N. Subsequent grid sizes are then defined by $N_{n+1} := \max(N_n - 1, N_{\min})$ for $n > 0$. Note that a minimum grid size $N_{\min} \in \mathbb{N}$ is crucial to maintain viability. In theory, if the first solution is feasible, all subsequent solutions are feasible for $N_n \to 1$. However, any small disturbance results in a potential loss of viability for small grid sizes in practice. It is well known that systems often require multiple switches in control to reach x_f, even for initial states close to x_f. For unconstrained linear systems, [13], [24] suggest to choose $N_{\min} \geq p/q$ with state dimension p and control dimension q respectively. A proper value for $N_{\min}$ depends on the system and constraint sets, however, choosing some $N_{\min} > p$ is a good starting point for simulations and experiments.

Taking the grid adaption into account, control law (6) for $t_\mu \in [t_{\mu,n}, t_{\mu,n} + \Delta t_{\mu,n})$ with $\Delta t_{\mu,n} := \Delta t^*\big(x_\mu(t_{\mu,n}), N_n\big)$ results in:

$$\mu\big(x_\mu(t_\mu)\big) := u^*\big(0, x_\mu(t_{\mu,n}), N_n\big). \tag{10}$$

In addition, choosing $\Delta t_{\min} > 0$ appropriately circumvents the numerical ill-conditioning and zero interval lengths $\Delta t_{\mu,n} = 0$ for states inside $\mathbb{X}_f$. However, as soon as $\Delta t^*(x_\mu, N) = \Delta t_{\min}$ for some x_μ and N is reached, i.e. for $x_\mu \in P_c(N, N\Delta t_{\min})$, the cost in (5) remains constant which in turn affects closed-loop convergence.

Figure 2 shows the different stages during closed-loop control depending on $N_{\min}$ and $\Delta t_{\min}$. As long as $N_n > N_{\min}$ lasts, the closed-loop evolution coincides with the initially predicted trajectories. Afterward, as soon as $N_n = N_{\min}$ is reached, the controller takes one more step with $\Delta t_{\mu,n} = \Delta t^*(x_s, N)$ before the temporal resolution increases and hence loosing recursive feasibility guarantees. For the active lower bound $\Delta t^*(\cdot, N_n) = \Delta t_{\min}$ (third stage), the cost function remains constant and hence asymptotic stability can no longer be maintained. These observations are captured by the following results:

Lemma 1: Let $t_f^*(x_s, N) \in \mathbb{R}^+$ denote the optimal transition time obtained from (5) with $x_s \in \mathbb{X}$, $\mathbb{X}_f = \{x_f\}$ and grid size $N \geq 1$. Further assume that the solution is feasible. Then, relation

$$t_f^*(x_s, N) > N\Delta t_{\min} \iff x_s \notin P_c(N, N\Delta t_{\min}) \tag{11}$$

holds for $\Delta t_{\min} \geq 0$.

Proof: First, we abbreviate $t_f^* := t_f^*(x_s, N)$, define $t_{\min} := N\Delta t_{\min}$ and consider the case $x_s \notin P_c(N, t_{\min}) \implies t_f^* > t_{\min}$. The implication follows immediately from the definition of $P_c(N, t_{\min})$ even for non-optimal t_f. By contraposition, the implication is equivalent to $t_f^* \leq t_{\min} \implies x_s \in P_c(N, t_{\min})$. The optimal solution is feasible by assumption and hence $\mathscr{U}^N(x_s, t_f^*) \neq \emptyset$ and $t_f^* \geq t_{\min}$ are ensured such that condition $t_f^* \leq t_{\min}$ is replaced by $t_f^* = t_{\min}$. Consequently, all requirements for $x_s \in P_c(N, t_{\min})$ are met.

The second case $t_f^* > t_{\min} \implies x_s \notin P_c(N, t_{\min})$ does not hold for arbitrary (non-optimal) t_f since control trajectories $u \in \mathscr{U}^N(x_s, t_f)$ could exists which start and end in $P_c(N, t_{\min})$ but fulfill $t_f^* > t_{\min}$ (for example keeping the system at the steady state). However, to show that the implication holds for t_f^* subject to (5), consider the contraposition $x_s \in P_c(N, t_{\min}) \implies t_f^* \leq t_{\min}$. If $x_s \in P_c(N, t_{\min})$ holds, then $\mathscr{U}^N(x_s, t) \neq \emptyset$ for $0 \leq t \leq t_{\min}$ by Definition 1. Solving (5) results in minimum-time solutions adhering to constraint $t_{\min} \leq t_f^*$ and hence the only feasible transition time for $x_s \in P_c(N, t_{\min})$ is $t_f^* = t_{\min}$. The existence of this particular $u \in \mathscr{U}^N$ is confirmed by assumption (feasibility). Consequently, $t_f^* = t_{\min}$ proves the original implication $x_s \in P_c(N, t_{\min}) \implies t_f^* \leq t_{\min}$.

Finally, equivalence (11) follows immediately since both implications are true. ∎

Proposition 1: Consider system (1) with initial state $x_s \in \mathbb{X}$, final state $\mathbb{X}_f = \{x_f\}$, optimal control problem (5) and control law (10). Choose $N_{\min} \geq 1$ and define $\Delta t_{\min} \geq 0$ and $N \geq N_{\min}$ ensuring $\Delta t_{\min} < \Delta t^*(x_s, N)$. Furthermore, assume that the initial solution to (5) is feasible. Then, the closed-loop system reaches the region $P = P_c\big(N_{\min}, (N_{\min}-1)\Delta t^*(x_s, N)\big)$.

Proof: The proof relies on the dynamic programming principle [21] and hence its mathematical exposition is kept brief. Let P abbreviate $P := P_c\big(N_{\min}, (N_{\min}-1)\Delta t^*(x_s, N)\big)$, x_μ the current state $x_\mu := x_\mu(t_{\mu,n})$ and x_μ^+ the successor state $x_\mu^+ := \varphi_\mu\big(t_{\mu,n+1}, t_{\mu,n}, x_\mu(t_{\mu,n})\big)$. The solution to the first optimal control problem at time $t_{\mu,0}$ is feasible by assumption and hence an admissible control trajectory $u \in \mathscr{U}^N(x_s, t_f^*(x_s, N))$ exists. Note that the grid is adapted with $N_0 := N$ and $N_{n+1} := \max(N_n - 1, N_{\min})$. First, consider the case $N_n > N_{\min}$. The optimal cost function value is $V(x_\mu) = t_f^*(x_\mu, N_n)$. Applying the principle of optimality results in

$$\begin{aligned} t_f^*(x_\mu, N_n) &= \Delta t^*(x_\mu, N_n) + (N_n - 1)\Delta t^*(x_\mu, N_n) \\ &= \Delta t^*(x_\mu, N_n) + (N_n - 1)\Delta t^*(x_\mu^+, N_n - 1) \\ \Leftrightarrow V(x_\mu) &= \Delta t^*(x_\mu, N_n) + V(x_\mu^+). \end{aligned} \quad (12)$$

Consequently, the solution at x_μ^+ with grid size $N_n - 1$ coincides with the previous solution, and hence the nominal closed-loop and open-loop evolution are identical. This includes recursive feasibility which implies forward invariance as well as the control to P. It can be easily verified that (12) only holds as long as N_n can be reduced by one in each step. $N_n \geq N_{\min} > 0$ is ensured by definition. As soon as $N_n = N_{\min}$ is reached, control law (10) performs one more step with $\Delta t^*(x_s, N_n)$. Afterward, $\Delta t^*(x_\mu, N_{\min})$ decreases in

each step (see Figure 2) so it does not match the optimal cost value in the previous step, invalidating (12). ∎

Condition $\Delta t_{\min} < \Delta t^*(x_s, N)$ ensures that the closed-loop state is not inside $P_c(N_{\min}, N_{\min}\Delta t_{\min})$ before the systems enters P and applies for proper choices of $\Delta t_{\min}$ and N (Lemma 1). Note, Proposition 1 even holds for $\Delta t_{\min} \leq \Delta t^*(x_s, N)$, however, we exclude this case to avoid ambiguous non-time optimal solutions as described before. For arbitrary systems, Proposition 1 does not guarantee true practical stability, i.e. that the state is ultimately bounded to P after arrival.

Practical implications of these results are that by increasing the initial N, which in turn reduces $\Delta t^*(\cdot, \cdot)$, or by decreasing $N_{\min}$, the size of region P is reduced. In contrast, certain choices of N and $N_{\min}$ are further implicitly bounded by $\Delta t_{\min}$, viability and the computational resources, thus limiting the endless decrease of P. However, the specific control applications then decide if this particular region is small enough to, for example, realize a proper point-to-point motion. Alternatively, it facilitates the systematic design of a dual-mode controller as described in Section V.

Remark 2: Recursive feasibility does not generally hold for adaptation schemes that adjust the grid resolution w.r.t. a desired sample time $\Delta t_s \in \mathbb{R}^+$ as in [18]. However, these schemes are particularly interesting in applications for which viability is assumed for the whole state space and for changes in x_f. An extended adaptation strategy with hysteresis $\Delta t_\epsilon \in \mathbb{R}_0^+$ is given as follows:

$$\begin{aligned} \Delta t_n^* &:= \Delta t^*\big(x_\mu(t_{\mu,n}), N_n\big), \\ N_{n+1} &= \begin{cases} \max\big(\Phi(\Delta t_n^*, N_n), N_{\min}\big) & |\Delta t_n^* - \Delta t_s| > \Delta t_\epsilon \\ \max(N_n - 1, N_{\min}) & \text{otherwise} \end{cases}. \end{aligned}$$

Temporal adaption in $\Phi(\Delta t_n^*, N_n)$ could be achieved by estimation, i.e. $\Phi(\Delta t_n^*, N_n) = \min(N_n \Delta t_n^*/\Delta t_s, N_{\max})$ and $N_{\max} \in \mathbb{N}$ as safeguard, or by linear search $\Phi(\Delta t_n^*, N_n) = N_n + 1$ for $\Delta t_n^* > \Delta t_s + \Delta t_\epsilon$ resp. $\Phi(\Delta t_n^*, N_n) = N_n - 1$ for $\Delta t_n^* < \Delta t_s - \Delta t_\epsilon$. By setting $\Delta t_s = \Delta t^*(x_s, N)$, adaptation is inactive and hence convergence holds according to Proposition 1 and since $|\Delta t_n^* - \Delta t_s| \leq \Delta t_\epsilon$ holds for all n outside P.

IV. DIRECT TRANSCRIPTION

A. Formulation

This section addresses the realization of optimal control problem (5) in terms of two different nonlinear program formulations that retain the inherent sparse structure of standard MPC. The first formulation is referred to as global uniform grid approach. Let Δt, u_k with $k = 0, 1, \ldots, N - 1$ and x_k with $k = 0, 1, \ldots, N$ denote the parameters subject to optimization. Accordingly, the nonlinear program is defined

as follows:

$$\min_{\substack{u_0,u_1,\ldots,u_{N-1},\\ x_0,x_1,\ldots,x_N,\\ \Delta t}} N\Delta t \qquad (13)$$

subject to

$$x_0 = x_{\mathrm{s}}, \quad x_N \in \mathbb{X}_{\mathrm{f}}, \quad x_k \in \mathbb{X}, \quad u_k \in \mathbb{U},$$
$$\Delta t_{\min} \leq \Delta t \leq \Delta t_{\max}, \quad x_{k+1} = \varphi(\Delta t, x_k, u_k),$$
$$k = 0, 1, \ldots, N-1.$$

Local optimization solvers often assume that $\mathbb{X}, \mathbb{U}$ and $\mathbb{X}_{\mathrm{f}}$ are compact and convex. In every practical implementation these sets are replaced by algebraic equality and inequality constraint functions which is usually straightforward and not described here in detail. Note that the sparsity pattern of the Hessian of Lagrangian, e.g., contains a single dense row and column for the parameter Δt. Another nonlinear program that is larger, though sparser, results from the definition of individual Δt_k and a uniformity condition $\Delta t_k = \Delta t_{k+1}$:

$$\min_{\substack{u_0,u_1,\ldots,u_{N-1},\\ x_0,x_1,\ldots,x_N,\\ \Delta t_0,\Delta t_1,\ldots,\Delta t_{N-1}}} \sum_{k=0}^{N-1} \Delta t_k \qquad (14)$$

subject to

$$x_0 = x_{\mathrm{s}}, \quad x_N \in \mathbb{X}_{\mathrm{f}}, \quad x_k \in \mathbb{X}, \quad u_k \in \mathbb{U},$$
$$\Delta t_{\min} \leq \Delta t_0 \leq \Delta t_{\max}, \quad \Delta t_k = \Delta t_{k+1},$$
$$x_{k+1} = \varphi(\Delta t_k, x_k, u_k), \quad k = 0, 1, \ldots, N-1.$$

This formulation is referred to as local uniform grid approach.

Proposition 2: The solutions to optimal control problems (5), (13) and (14) are identical.

Proof: Even if the proof is mostly trivial, we include it for the sake of completeness. First, we show that optimal control problems (5) and (13) coincide and so does their solution. The control function space $\mathscr{U}^N(x_{\mathrm{s}}, t_{\mathrm{f}}) \subseteq \mathcal{U}^N(t_{\mathrm{f}})$ is defined according to a uniform grid with size N and partition length Δt. Accordingly, $t_{\mathrm{f}} = N\Delta t$ defines the cost function in (13). As the control trajectory is piecewise constant w.r.t. the grid, i.e. $u(t) := u_k$ for $t \in [t_k, t_k + \Delta t)$, it is completely described by parameters u_k with $k = 0, 1, \ldots, N-1$ and Δt. To account for the admissibility conditions in $\mathscr{U}^N(x_{\mathrm{s}}, t_{\mathrm{f}})$, let $x_k := \varphi(kt_{\mathrm{f}}/N, x_{\mathrm{s}}, u(t))$ denote the states at grid points t_k. According to (2), it is $x_0 = x_{\mathrm{s}}$ and by time-invariance of (1) $x_{k+1} = \varphi(\Delta t, x_k, u_k)$ for $k = 0, 1, \ldots, N-1$. Control constraints in $\mathscr{U}^N(x_{\mathrm{s}}, t_{\mathrm{f}})$ are imposed by enforcing $u_k \in \mathbb{U}$ and state constraints at grid points by $x_k \in \mathbb{X}$ for $k = 0, 1, \ldots, N-1$. The last state must adhere to $x_N = \varphi(t_{\mathrm{f}}, x_{\mathrm{s}}, u(t)) \in \mathbb{X}_{\mathrm{f}}$. By uniformity, $N\Delta t_{\min} \leq t_{\mathrm{f}} \leq N\Delta t_{\max}$ is substituted by $\Delta t_{\min} \leq \Delta t \leq \Delta t_{\max}$. Consequently, minimizing (13) w.r.t. all u_k, all x_k and Δt leads to the same solution as (5).

Showing that the solutions to (13) and (14) coincide is straightforward. Equality constraint $\Delta t_k = \Delta t_{k+1}$ in (14) ensures uniformity for the optimal solution such that $\Delta t_k^*(x_{\mathrm{s}}, N) = \Delta t^*(x_{\mathrm{s}}, N)$ holds for all $k = 0, 1, \ldots, N-1$ and hence the minimum cost is $\sum_{k=0}^{N-1} \Delta t_k^*(x_{\mathrm{s}}, N) = N\Delta t^*(x_{\mathrm{s}}, N)$ which coincides with (13). The same applies to constraints. ∎

Necessary and sufficient optimality conditions for general nonlinear programs apply [25]. Note that the deflection constraint $x_{k+1} = \varphi(\Delta t_k, x_k, u_k)$ in (13) and (14) is continuously differentiable w.r.t. $\Delta t_k, x_k, u_k$ and x_{k+1} even though the grid is temporally variable. Any practical realization solves the initial value problem (2) numerically, e.g. by one-step methods (Euler, Runge-Kutta) that maintain continuous differentiability. Hereby, the theory of sampled-data systems applies which usually requires fast sampling [26]. By choosing the Euler family or the implicit trapezoidal rule, i.e. $\varphi(\Delta t_k, x_k, u_k) \approx x_k + \Delta t_k f(x_k, u_k)$ for forward Euler, an interesting nominal asymptotic stability result follows under certain conditions:

Proposition 3: Consider system (1) with initial state $x_{\mathrm{s}} \in \mathbb{X}$, optimal control problem (13) or (14), control law (10) and Euler resp. trapezoidal integration. Let $\mathbb{X}_{\mathrm{f}} = \{x_{\mathrm{f}}\}$ represent a steady state such that there exists $u \in \mathbb{U}$ with $f(x_{\mathrm{f}}, u) = 0$. Choose $N_{\min} = 1$ and define $\Delta t_{\min} > 0$ and $N \geq 1$ ensuring $\Delta t_{\min} < \Delta t^*(x_{\mathrm{s}}, N)$. Furthermore, assume that the initial solution is feasible and that constraint qualifications as well as second-order necessary conditions hold. Then, the closed-loop system is asymptotically stable on $\mathbb{X}$.

Proof: The proof is based on Proposition 1. Since the minimum grid size is set to $N_{\min} = 1$, the principle of optimality ensures that the system actually reaches $P = P_c(N_{\min}, (N_{\min} - 1)\Delta t^*(x_{\mathrm{s}}, N)) = x_{\mathrm{f}}$. As soon as the grid reduces to $N = N_{\min}$ for some $x_\mu(t_{\mu,n})$ the successor state is $x_\mu(t_{\mu,n+1}) = x_{\mathrm{f}}$. Due to $N_{\min} = 1$ and condition $\Delta t_{\min} < \Delta t^*(x_{\mathrm{s}}, N)$, the system reaches x_{f} before the optimal time interval reduces to $\Delta t_{\min}$. Since $\Delta t_{\min} > 0$, the KarushKuhnTucker conditions ensure recursive feasibility and nominal asymptotic stability beyond x_{f}: The set $\mathbb{U}$ is replaced by an algebraic description in any practical realization (see Section IV). Let this set defined by $g(u_0) \leq 0$ with $g : \mathcal{U} \mapsto \mathbb{R}^S$. State restrictions $\mathbb{X}$ are fulfilled implicitly since $N = 1$ and initial respectively final states are fixed to x_{f}.

We show now that first-order optimality conditions (see [25]) ensure to find $u_0^* \in \mathbb{U}$ such that $f(x_{\mathrm{f}}, u_0^*) = 0$ holds. Since $N = 1$, states are directly substituted and the remaining optimization parameters are u_0 and $\Delta t_k = \Delta t = t_{\mathrm{f}}$. Applying the forward Euler method to (2) results in the equality constraint $h(u_0, \Delta t) := x_{\mathrm{f}} - x_{\mathrm{f}} + \Delta t f(x_{\mathrm{f}}, u_0) = 0$.

The Lagrangian with multipliers $\lambda_0 \in \mathbb{R}^p$, $\mu_0 \in \mathbb{R}^S$ and $\mu_1 \in \mathbb{R}$ is given by $\mathcal{L}(u_0, \Delta t, \lambda_0, \mu_0, \mu_1) = \Delta t + \lambda_0^\mathsf{T} h(u_0, \Delta t) + \mu_0^\mathsf{T} g(u_0) + \mu_1(\Delta t_{\min} - \Delta t)$. The first-order optimality conditions for the optimal parameters (indicated by a star) are:

$$\nabla_{u_0} \mathcal{L}(\cdot) = \nabla_{u_0}\left(\lambda_0^{*\mathsf{T}} h(u_0^*, t_{\mathrm{f}})\right) \qquad (15a)$$
$$+ \nabla_{u_0}\left(\mu_0^{*\mathsf{T}} g(u_0^*)\right) = 0, \qquad (15b)$$
$$\nabla_{\Delta t} \mathcal{L}(\cdot) = 1 + \lambda_0^\mathsf{T} f(x_{\mathrm{f}}, u_0^*) - \mu_1^* = 0, \qquad (15c)$$
$$h(u_0^*, \Delta t^*) = 0, \qquad (15d)$$
$$\mu_0^{*\mathsf{T}} g(u_0^*) = 0, \qquad (15e)$$
$$\mu_1^*(\Delta t_{\min} - \Delta t^*) = 0, \qquad (15f)$$
$$g(u_0^*) \leq 0, \ \Delta t^* \geq \Delta t_{\min}, \ \mu_0^* \geq 0, \ \mu_1^* \geq 0. \qquad (15g)$$

Parameter $\Delta t^* \geq \Delta t_{\min} > 0$ is strictly positive by definition. Consequently, (15d) ensures that u_0^* satisfies $f(x_{\mathrm{f}}, u_0^*) = 0$
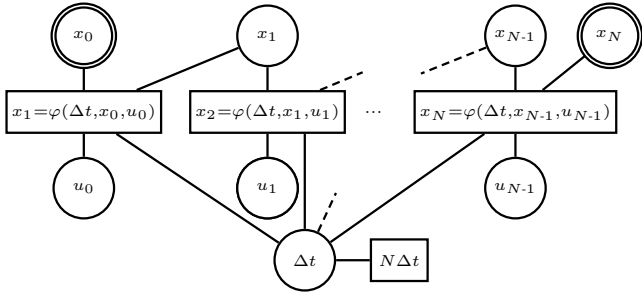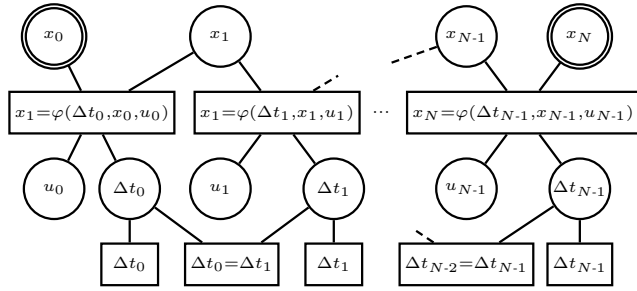
Fig. 3: Hypergraph of the global uniform grid

Fig. 4: Hypergraph of the local uniform grid

(a) Global uniform grid   (b) Local uniform grid

Fig. 5: Structure of the Hessian of the Lagrangian for a second order system with $N = 10, p = 2$ and $q = 1$.

and that particular u_0^* exists by definition and $g(u_0^*) \leq 0$ holds. Combining (15c) and $f(x_{\mathrm{f}}, u_0^*) = 0$ implies $\mu_1^* = 1$ which in turn confirms with (15f) that the optimal time interval Δt^* satisfies $\Delta t^* = \Delta t_{\min}$. Equations (15b) and (15e) are fulfilled by proper choices of λ_0^* and μ_0^*. For example, if control constraints $g(\cdot)$ are inactive, $\mu_0^* = \lambda_0^* = 0$ are possible solutions. For the other one-step methods, i.e. backward Euler and trapezoidal rule, $h(u_0^*, \Delta t^*) = 0$ also immediately implies $f(x_{\mathrm{f}}, u_0^*) = 0$ which is skipped for brevity.

Constraint qualification and second-order sufficient conditions for a true feasible (local) minimizer are ensured by assumption. ∎
The result inherently addresses recursive feasibility and hence ensures forward invariance on $\mathbb{X}$. Satisfying condition $\Delta t_{\min} < \Delta t^*$ is straightforward by a proper choice of N. However, the result is rather theoretical as $N_{\min} = 1$ is often required for robustness in practice (refer to the discussion in Section III).

B. Hypergraph Representation

The local and the global uniform grid reveal different sparsity patterns due to their optimization structure. This is also immediately visible in its hypergraph representation as introduced for MPC in [27]. A hypergraph is a graph composed of a set of vertices and a set of hyperedges. Hyperedges connect an arbitrary number of vertices rather than only pairs of vertices compared to regular graphs. For nonlinear programs (13) and (14), each vertex refers to an optimization parameter, i.e. x_k, u_k or Δt_k. A hyperedge refers to cost or constraint terms and is only connected to the nodes on which they directly depend. Figure 3 shows the hypergraph for the global uniform grid (13). Trivial substitutions for optimization parameters like $x_0 = x_{\mathrm{s}}$ are not represented by a dedicated edge as these parameters are not subject to optimization. These
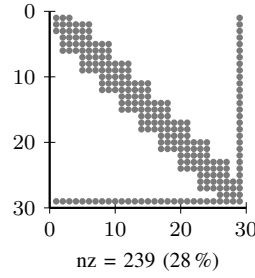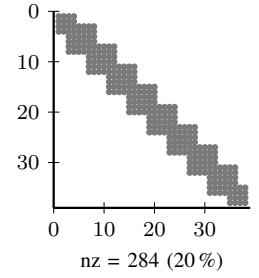
vertices are called fixed which is indicated by a double circle. Also lower and upper bounds for optimization parameters are directly cached in their vertices. Note that parameter Δt in Figure 3 is connected with all edges for adhering to the system dynamics. This indicates a dense column in the constraint Jacobian respectively a dense row and column in the Hessian of the Lagrangian (see Figure 5a). In contrast, the hypergraph for the local uniform grid (14) contains more vertices, but the maximum number of connected vertices for each edge is limited and independent of N. Figure 5b shows an example for the corresponding structure of the Hessian of the Lagrangian in which the percentage of non-zeros (nz) is smaller.

The hypergraph representation is well suited for the practical implementation. It allows efficient computations of derivatives based on sparse finite differences. The graph eliminates the need for an extra graph coloring algorithm to find the sparsity patterns. Block Jacobian and Hessian matrices are straightforward to calculate by iterating edges or vertices in the graph. Furthermore, the grid size adaptation as described in Section III leads to the ongoing change of problem dimensions. Reconfiguring the hypergraph online while maintaining the inherent sparse structure requires almost negligible overhead which is crucial for real-time control. Refer to [27] for a detailed description and general performance results.

V. QUASI-TIME-OPTIMAL DUAL-MODE CONTROL

As mentioned before, the results summarized in Proposition 1 facilitate the dual-mode controller design. Dual-mode MPC is the predecessor to quasi-infinite horizon MPC concerning stability enforcement [28]. The key idea is to control the system to a terminal region $\mathbb{X}_{\mathrm{lin}}$ and then switch to an external local stabilizing controller [29], [30]. In addition, stabilization with the dual-mode realization does not suffer from extensive chattering like actual time-optimal controllers do.

Let x_{f} denote the steady state at which the system should be stabilized and u_{f} the corresponding control such that $f(x_{\mathrm{f}}, u_{\mathrm{f}}) = 0$ holds. Assume that the linearized system $\dot{x}_{\mathrm{lin}}(t) = A_c x_{\mathrm{lin}}(t) + B_c u_{\mathrm{lin}}(t)$ with $A_c := \mathrm{D}_x f(x_{\mathrm{f}}, u_{\mathrm{f}})$ and $B_c := \mathrm{D}_u f(x_{\mathrm{f}}, u_{\mathrm{f}})$ is stabilizable. Then, a linear state feedback $K \in \mathbb{R}^{q \times p}$ can be determined such that $A_c - B_c K$ is asymptotically stable. However, since the original plant is nonlinear and constraints are present, the region of operation is

limited to some set $\mathbb{X}_{\text{lin}} \subseteq \mathbb{X}$. The set $\mathbb{X}_{\text{lin}}$ is determined such that the local feedback law $\mu_{\text{lin}}(x_\mu(t_\mu)) = K(x_{\text{f}} - x_\mu(t_\mu)) + u_{\text{f}}$ is admissible with $\mu_{\text{lin}}(x_\mu) \in \mathbb{U}$ for all $x_\mu \in \mathbb{X}_{\text{lin}}$. Furthermore, the closed-loop system must be rendered forward invariant, in particular $\varphi(t_\mu, x_{\text{s}}, \mu(x_\mu(t_\mu))) \in \mathbb{X}_{\text{lin}}$ for all $x_{\text{s}} \in \mathbb{X}_{\text{lin}}$ and $t_\mu \geq 0$. These requirements on $\mathbb{X}_{\text{lin}}$ ensure feasibility. However, to also ensure asymptotic stability, $\mathbb{X}_{\text{lin}}$ is further limited to provide a sufficient decrease of a suited Lyapunov function for the nonlinear closed-loop system. For a profound description refer to [30], [31].

Combining the control law from the linear controller design above with (10) results in the following quasi-time-optimal dual-mode control law:

$$\mu_{\text{dual}}(x_\mu(t_\mu)) = \begin{cases} \mu(x_\mu(t_\mu)) & \text{for } x_\mu(t_\mu) \notin \mathbb{X}_{\text{lin}} \\ \mu_{\text{lin}}(x_\mu(t_\mu)) & \text{for } x_\mu(t_\mu) \in \mathbb{X}_{\text{lin}} \end{cases} . \quad (16)$$

Remark 3: The sampling rate of μ_{lin} is subject to the local controller design. A practical realization might also consider a discrete-time LQR (see Section VI).

In order to ensure feasibility of the combined control law, $\mathbb{X}_{\text{f}} \subseteq \mathbb{X}_{\text{lin}}$ must hold, since otherwise the time-optimal controller would not reach $\mathbb{X}_{\text{lin}}$. Accordingly, even $P_c(N_{\min}, (N_{\min} - 1)\Delta t^*(x_{\text{s}}, N)) \subseteq \mathbb{X}_{\text{lin}}$ must hold to ensure a proper convergence to $\mathbb{X}_{\text{lin}}$:

Corollary 1: Consider the closed-loop control system and the assumptions according to Proposition 1 with design parameters $N, N_{\min}$ and $\Delta t_{\min}$. The resulting control law is denoted by $\mu(x_\mu)$. Furthermore, consider that a control law $\mu_{\text{lin}}(x_\mu)$ exists which ensures asymptotic stability and forward invariance for the nonlinear system for all states $x_\mu \in \mathbb{X}_{\text{lin}}$. Then, the closed-loop control system with composite control law (16) and steady state x_{f} is asymptotically stable on $\mathbb{X}$ if $P_c(N_{\min}, (N_{\min} - 1)\Delta t^*(x_{\text{s}}, N)) \subseteq \mathbb{X}_{\text{lin}}$ holds.

Proof: The closed-loop system according to Proposition 1 converges to $P_c(N_{\min}, (N_{\min} - 1)\Delta t^*(x_{\text{s}}, N))$ by ensuring recursive feasibility. By assumption, the local linear controller ensures forward invariance and asymptotic stability on $\mathbb{X}_{\text{lin}}$. Since control law (16) switches to the local controller as soon as $\mathbb{X}_{\text{lin}}$ is reached, condition $P_c(N_{\min}, (N_{\min} - 1)\Delta t^*(x_{\text{s}}, N)) \subseteq \mathbb{X}_{\text{lin}}$ immediately ensures that x_{f} is asymptotically stable for the whole dual-mode control system. ∎

VI. NUMERICAL EXAMPLE AND EVALUATION

In the following, a numerical example demonstrates the presented time-optimal control techniques. The Van der Pol oscillator constitutes a second-order dynamic system with non-linear damping and is commonly reported in the literature as benchmark system for control resp. system analysis methods. Its dynamics are described by $\ddot{y}(t) - (1 - y(t)^2)\dot{y}(t) + y(t) = u(t)$ with $y: \mathbb{R} \mapsto \mathbb{R}$. By defining the state vector $x(t) := (x_1(t), x_2(t))^\mathsf{T}$, the nonlinear control-affine state space model according to (1) is given by:

$$\begin{aligned} \dot{x}(t) &= f(x(t), u(t)) \\ &= (x_2(t), \ (1 - x_1(t)^2)x_2(t) - x_1(t) + u(t))^\mathsf{T}. \end{aligned} \quad (17)$$

Hereby, the unrestricted state and control sets are $\mathcal{X} = \mathbb{R}^2$ and $\mathcal{U} = \mathbb{R}$. For a given control reference $u_{\text{f}} \in \mathcal{U}$, the system
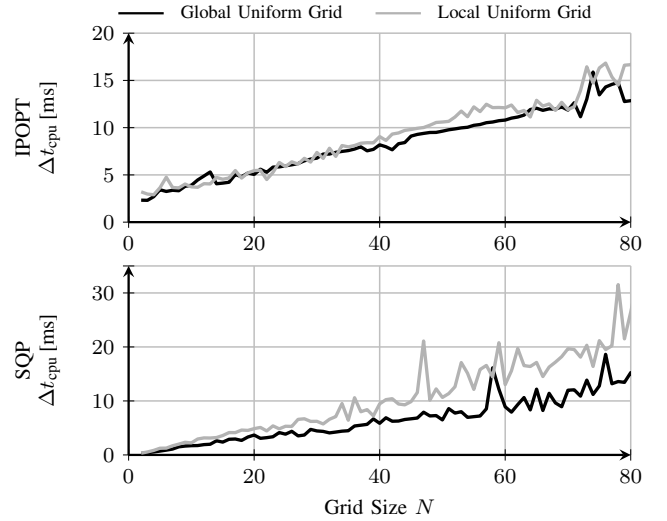
Fig. 6: Comparison of the grids with forward Euler for the Van der Pol oscillator. IPOPT with explicit Hessian computation is shown at the top and SQP at the bottom.

exhibits a unique steady state at $x_{\text{f}} = (u_{\text{f}}, 0)^\mathsf{T}$. Refer to [32] for a detailed control synthesis. In the following, the constraint sets are set to $\mathbb{X} = \mathcal{X}$ and $\mathbb{U} = \{u \in \mathcal{U} \mid |u| \leq 1\}$ respectively.

A. Open-Loop Control

This section investigates open-loop control in terms of a comparative analysis. Boundary values for the optimal control task are set to $x_{\text{s}} = (0, 0)^\mathsf{T}$ and $x_{\text{f}} = (0.8, 0)^\mathsf{T}$. The solution to the initial value problem (1) with system (17) is approximated with forward Euler.

The first analysis compares the global and local uniform grid performances for two different solver configurations that both exploit sparsity using the hypergraph and internal sparse algebra. In the first configuration, the nonlinear programs are solved by the sparse interior point solver IPOPT [33] and HSL-MA57 as internal linear solver [34]. The Jacobian is computed via sparse finite differences and a step width of $1 \cdot 10^{-9}$. Note that we also compute the explicit Hessian of the Lagrangian with two consecutive Jacobians and step width $1 \cdot 10^{-2}$. The second configuration is based on a sequential quadratic programming (SQP) approach. The underlying quadratic program solver is the sparse general purpose solver OSQP [35]. Our SQP method squares objective terms Δt_k in (14) resp. Δt in (13) and utilizes the Hessian of the objective rather than the Hessian of the Lagrangian. This procedure ensures positive definiteness of the Hessians required for OSQP without changing the actual minimizer. Furthermore, it speeds up computation times since additional constraint evaluations are omitted. The source code is available as part of our open-source C++ predictive control framework [36]. Figure 6 shows the median computation times for both grid realizations and varying grid size N (Ubuntu 16.04, Intel Core i7-4770 CPU at 3.4 GHz, 8 GB RAM, 20 repetitions). The computation times are almost comparable. For SQP, the global uniform grid performs slightly better. It is noticeable

TABLE I: Open-loop solving times in ms and integral errors for the Van der Pol oscillator with varying grid sizes N. The reference grid size which corresponds to $\Delta t \approx 0.1\,$s is indicated by N^*.

	$N = 5$		$N^* = 16$		$N = 25$		$N = 50$	
	Δt_{cpu}	$e_{\hat{x}}$	Δt_{cpu}	$e_{\hat{x}}$	Δt_{cpu}	$e_{\hat{x}}$	Δt_{cpu}	$e_{\hat{x}}$
TOMPC	135.27	0.06	13.88	0.06	49.25	0.06	174.16	0.06
ℓ_1-Norm ($\theta = 1.01$)	—	—	4.05	0.04	7.38	0.04	9.88	0.04
ℓ_1-Norm ($\theta = 1.1$)	—	—	4.46	0.04	6.14	0.04	12.88	0.04
ℓ_1-Norm ($\theta = 1.5$)	—	—	8.81	0.04	9.91	0.04	30.12	0.04
Local Grid	3.18	0.07	3.52	0.04	4.45	0.02	7.58	≈ 0

that due to the hypergraph the computation time increases almost linearly with the grid size.

The second analysis compares the proposed method with the state of the art approaches TOMPC and the ℓ_1-norm approach as mentioned in Section I. The control task is as before and the local uniform grid is selected as the candidate for variable discretization. TOMPC and the ℓ_1-norm approach are configured with a fixed grid of resolution $\Delta t = 0.1\,$s. Recall that TOMPC adapts the grid size N until the (quasi) minimum-time feasible solution is found which is for $N^* = 16$ in this scenario. Similarly, the ℓ_1-norm approach requires at least a grid size of $N^* = 16$ to return feasible solutions. An advantage of the proposed variable discretization methods is that they may return a feasible solution even for $N < N^*$ while reducing accuracy. To highlight this effect, we define an integral dynamics error w.r.t. the optimal solution x_{ref} obtained from a large grid resolution: $e_{\hat{x}} = \int_0^{t_{\text{f}}^*} \|x_{\text{ref}}(\tau) - \varphi(\tau, x_{\text{s}}, u^*(\tau))\|_2 \, \mathrm{d}\tau$. Table I lists the medians of the computation times and dynamic errors for the IPOPT solver configuration. Note that the ℓ_1-norm approach requires to choose a design parameter θ [5]. Choosing θ too large leads to fast growing values in the cost function which results in ill-conditions problems especially for large N and hence larger computation times. The local uniform grid reveals the lowest computation times for all grid sizes in this scenario.

B. Closed-Loop Control with Dual-Mode

This section investigates stabilizing closed-loop control with dual-mode. The grid size is set to $N = 50$ and $N_{\min} = 3$ serves as lower bound for the grid adaptation. Setting $\Delta t_{\max} = 0.05\,$s ensures the desired accuracy of the dynamics approximation and hence restricts the feasible state space for initial state x_{s} to $x_{\text{s}} \in P_c(N, N\Delta t_{\max})$. To account for a minimum grid resolution and closed-loop sampling times, $\Delta t_{\min}$ is set to $\Delta t_{\min} = 1 \cdot 10^{-3}\,$s. The control task consists of reaching steady state $x_{\text{f}} = (0,0)$ from three different initial states $x_{\text{s}} \in \{(-1.04, 0.56)^{\mathsf{T}}, (0.1, -0.5)^{\mathsf{T}}, (0.6, 0.6)^{\mathsf{T}}\}$.

For simplicity, the worst-case region of convergence $P = P_c(N_{\min}, (N_{\min} - 1)\Delta t_{\max})$ is determined by sampling the control and time space using the reverse-time formulation of system (17). Note that $\Delta t^*(x_{\text{s}}, N) \leq \Delta t_{\max}$ holds for all feasible initial states x_{s}. Sampling is performed according to a 4-dimensional grid with steps of length 0.1 in the control and $0.01\,$s for the transition time.

Dual-mode operation is achieved by choosing a discrete-time linear quadratic regulator (LQR) as secondary feedback controller. Hereby, we choose $\Delta t_{\text{LQR}} = \Delta t_{\min}$ as sample time. The design of the LQR requires a state error weighting matrix $R \in \mathbb{R}^{p \times p}$, a control error weighting matrix $Q \in \mathbb{R}^{q \times q}$ and a linear model $x_{k+1} = Ax_k + Bu_k$ which follows from linearizing the continuous-time model (17) at $x_{\text{f}} = (0,0)^{\mathsf{T}}$ and applying the zero-order hold method. The region of attraction $\mathbb{X}_{\text{lin}}$ is obtained by performing closed-loop simulations with the nonlinear system (17) and feedback $\mu_{\text{lin}}(x_\mu(t_\mu)) = -Kx_\mu(t_\mu)$ according to a predefined grid of resolution 0.2. $\mathbb{X}_{\text{lin}}$ is then set to the largest inscribed ellipse. Related parameters are listed below:

$$A = \begin{pmatrix} 1 & 0.001 \\ -0.001 & 1.001 \end{pmatrix}, B = \begin{pmatrix} 0 \\ 0.001 \end{pmatrix}, Q = \begin{pmatrix} 2 & 0 \\ 0 & 0.1 \end{pmatrix}, R = \begin{pmatrix} 0.1 \end{pmatrix},$$
$$K \approx \begin{pmatrix} 3.5737 & 3.8711 \end{pmatrix}, \mathbb{X}_{\text{lin}} = \{x \in \mathcal{X} \mid x^{\mathsf{T}} \begin{pmatrix} 16.65 & 14.03 \\ 14.03 & 18.19 \end{pmatrix} x \leq 1\}.$$

The linear system is controllable and hence stabilizable since (A, AB) has full row rank. Note that Q and R are chosen such that $\mathbb{X}_{\text{lin}}$ ensures $P \subseteq \mathbb{X}_{\text{lin}}$.

Figure 7 shows the closed-loop simulation results for both the full time-optimal and dual-mode realizations. In addition, Figure 7a visualizes the feasibility region $P_c(N, N\Delta t_{\max})$. The enlarged views in Figure 7b also highlight the practical stability region for $N_{\min} = 3$ and for comparison also $N_{\min} = 2$ (marked by P_2), which is significantly smaller. Note that choosing $N_{\min} = 3$ is rather conservative in this example with $p = 2$. The three full time-optimal realizations are still able to stabilize the system even though recursive feasibility cannot be guaranteed. In addition, the solution to (13) for states within the region of constant cost, i.e. for $x_\mu \in P_c(N_{\min}, N_{\min}\Delta t_{\min})$ results in $u_{\text{f}} := u^*(0, x_\mu, N_{\min}) = 0$ ensuring $f(x_\mu, u_{\text{f}}) = 0$. This does not hold for arbitrary systems and configurations (refer also to the proofs of Proposition 3). The dual-mode controller switches to different trajectories as soon as $\mathbb{X}_{\text{lin}}$ is reached and ensures asymptotic stability. Figure 8 depicts the evolution of control inputs associated with the closed-loop realizations. Notice that each full time-optimal realization reveals a peak in control before switching to u_{f}. These peaks occur within the region P as a result of the changed grid resolution and hence indicate potential recursive feasibility losses. The dual-mode realization inherently leads to longer transition times, however, further tuning of Q, R and N affecting the sizes of $\mathbb{X}_{\text{lin}}$ and P leads to more conservative respectively aggressive transitions. Note that asymptotic stability also holds if the controller switches in $\mathbb{X}_{\text{lin}} = P$ (as $P \subseteq \mathbb{X}_{\text{lin}}$), assuming forward invariance of P, which significantly reduces transition times.

VII. ECP INDUSTRIAL PLANT EMULATOR

This section investigates the closed-loop control on a real system as shown in Fig. 9. The *ECP Industrial Plant Emulator Model 220* consists of two load plates actuated by motors which motion is coupled by transmission belts. Angular position and angular velocity are estimated from encoder signals with a DSP.

In the experimental setup, both motors generate torques to regulate the position and velocity of the plate of the secondary
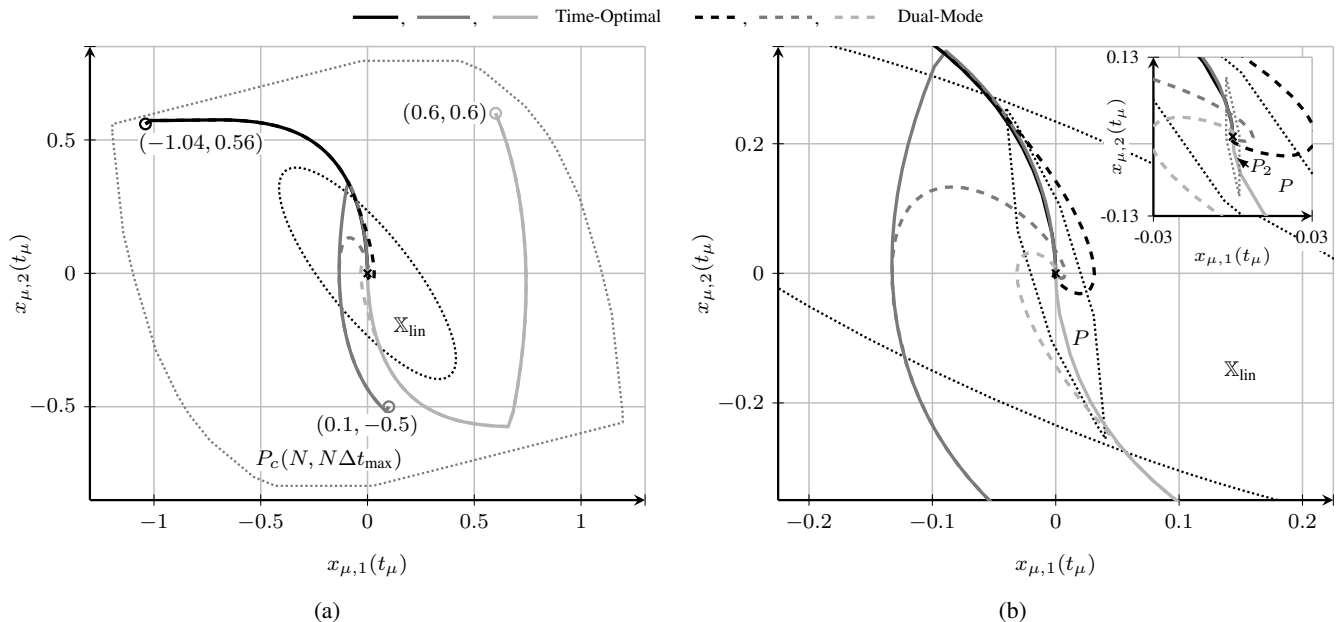
Fig. 7: Closed-loop results for the Van der Pol oscillator. (a) Three individual solutions with $N = 50$, $N_{\min} = 3$ and $\Delta t_{\max} = 0.05\,\mathrm{s}$ from different initial states (indicated by circles) are shown and the steady state $x_{\mathrm{f}} = (0,0)^{\mathsf{T}}$ is marked by a cross. $P = P_c\big(N_{\min}, (N_{\min} - 1)\Delta t_{\max}\big)$ denotes the worst-case practical stability region with $N_{\min} = 3$. (b) Magnified views for the vicinity of x_{f}. For comparison, P_2 indicates the practical stability region for $N_{\min} = 2$.
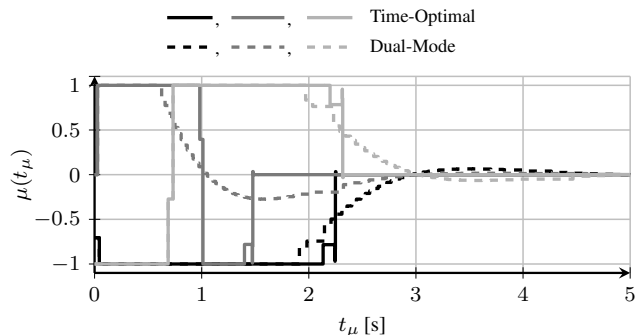
Fig. 8: Evolution of the control inputs for the closed-loop realizations described in Figure 7.
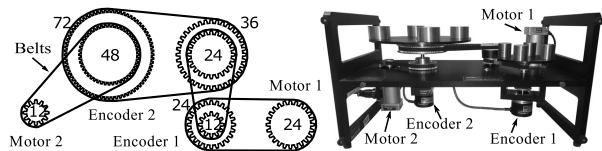
Fig. 9: ECP Industrial Plant Emulator Model 220

drive. The system is described by the following nonlinear differential equation:

$$\ddot{x}(t) = -c_1\dot{x}(t) - c_2 \tanh\big(c_3\dot{x}(t)\big) + k_1 u_1(t) - k_2 u_2(t) \quad (18)$$

with $k_1 = 34.51$, $k_2 = 34.13$, $c_1 = 1.46$, $c_2 = 2.53$ and $c_3 = 5$. Note, that $\tanh(\cdot)$ is chosen as a smooth approximation of the actual sign function. The optimal control problem is constructed as before with state vector $x(t) = (x(t), \dot{x}(t))^{\mathsf{T}}$, control bounds $|u_1(t)| \le 0.5$, $|u_2(t)| \le 0.5$ and velocity

bounds $|\dot{x}(t)| \le 5$.

The time optimal control task is specified with forward Euler integration, $\Delta t_{\mathrm{s}} = 0.05$, $\Delta t_{\min} = 0.001$, $N_{\min} = 2$ and $\mathbb{X}_{\mathrm{f}} = \{x_{\mathrm{f}}\}$ with $x_{\mathrm{f}} = (x_{\mathrm{f},1}, x_{\mathrm{f},2})^{\mathsf{T}}$. The ℓ_1-norm approach serves as reference with $N = 40$ to ensure feasibility for all transitions (TOMPC is not real-time capable in this scenario). The local uniform grid starts at $N = 20$ and the grid is adapted by linear search as described in Remark 2. Note that $x_{\mathrm{f},1}$ is subject to change during runtime. The dual-mode controller design is subject to the following parameters:

$$A = \begin{pmatrix} 0 & 1 \\ 0 & 12.63\tanh(5x_{\mathrm{f},2})-14.1 \end{pmatrix}, B = \begin{pmatrix} 0 & 0 \\ 34.51 & -34.13 \end{pmatrix},$$
$$R = \begin{pmatrix} 1 & 0 \\ 0 & 1 \end{pmatrix}, Q = \begin{pmatrix} 1 & 0 \\ 0 & 0.1 \end{pmatrix}, K \approx \begin{pmatrix} 0.711 & 0.131 \\ -0.703 & -0.130 \end{pmatrix},$$
$$\mathbb{X}_{\mathrm{lin}} = \{x \in \mathcal{X} \mid x^{\mathsf{T}}\begin{pmatrix} 2.2 & 0.38 \\ 0.38 & 0.11 \end{pmatrix}x \le 1\}.$$

Note that the linear approximation (A, B) does not depend on the angular reference position $x_{\mathrm{f},1}$. Therefore, $\mathbb{X}_{\mathrm{lin}}$ is translated to $x_{\mathrm{f}} = (x_{\mathrm{f},1}, 0)^{\mathsf{T}}$ whenever $x_{\mathrm{f},1}$ changes.

Figure 10 shows the control, state and computation time profiles for the different realizations and varying reference positions $x_{\mathrm{f},1}$. The closed-loop performance between the local uniform grid (without dual-mode) and the ℓ_1-norm approach is very similar which is reasonable because both claim to be time-optimal. According to the analysis in Section III, however, the controller does not guarantee stabilization, even if it is achieved here by chattering the control inputs. In contrast, the stabilizing quasi-time-optimal dual-mode realization performs quite similar at the beginning of each transition, but then lead to a smooth stabilization at x_{f}. Note that the drop in computation time (bottom plot) indicates when the LQR is active. In this scenario, the computation times are

Fig. 10: Closed-loop control of the ECP Model 220 with varying final position $x_{f,1}$. These are the local uniform grid, a dual-mode and hybrid cost realization and the ℓ_1-norm approach. Note, $\mu_2(\cdot)$ is omitted as it is similar to $-\mu_1(\cdot)$.

comparable, but they decrease for the local uniform grid due to grid adaptation.

VIII. CONCLUSION

Common time-optimal control formulations with state feedback, for example based on time transformation, do not take the control parameterization typically arising in MPC into account such that recursive feasibility and stabilization can no longer be guaranteed. To this end, this paper proposes a suitable formulation based on variable discretization and grid adaptation for which closed-loop convergence results are derived. Even though these results mainly deal with the nominal case, however, they include design parameters, i.e. lower bounds on the temporal resolution and the grid size, to inherently deal with numerical ill-conditioning and a potential loss of viability. In addition, a dual-mode control scheme results in a smooth quasi-time-optimal stabilization. From an implementation point of view, two proposed nonlinear program formulations result in the same optimal solution but reveal different sparsity patterns. Under more restricted conditions and a class of numerical integration schemes, these formulations also ensure true time-optimality and asymptotic stability without dual-mode. A numerical example demonstrates the design of the proposed schemes and provides a comparative analysis with state of the art approaches. Experimental results with a real system highlight the practical feasibility of the proposed method.

Future work investigates moving horizon time-optimal control schemes with terminal conditions that do not necessarily require a dedicated dual-mode design to asymptotically stabilize the system.

REFERENCES

[1] L. Grüne and J. Pannek, *Nonlinear Model Predictive Control: Theory and Algorithms*, 2nd ed., ser. Communications and Control Engineering. Springer, 2017.

[2] J. B. Rawlings, D. Q. Mayne, and M. M. Diehl, *Model Predictive Control: Theory, Computation, and Design*, 2nd ed. Nob Hill Publishing, 2017.

[3] V. H. Quintana and E. J. Davison, "A numerical method for solving optimal control problems with unspecified terminal time," *International Journal of Control*, vol. 17, no. 1, pp. 97–115, 1973.

[4] K. L. Teo, L. S. Jennings, H. W. J. Lee, and V. Rehbock, "The control parameterization enhancing transform for constrained optimal control problems," *The Journal of the Australian Mathematical Society. Series B. Applied Mathematics*, vol. 40, no. 3, pp. 314–335, 1999.

[5] R. Verschueren, H. J. Ferreau, A. Zanarini, M. Mercangöz, and M. Diehl, "A stabilizing nonlinear model predictive control scheme for time-optimal point-to-point motions," in *IEEE Conference on Decision and Control*, 2017, pp. 2525–2530.

[6] J. Zhao, M. Diehl, R. Longman, H. G. Bock, and J. P. Schlöder, "Nonlinear model predictive control of robots using real-time optimization," in *AIAA/AAS Astrodynamics Specialist Conference and Exhibit*, 2004.

[7] R. Verschueren, N. van Duijkeren, J. Swevers, and M. Diehl, "Time-optimal motion planning for n-dof robot manipulators using a path-parametric system reformulation," in *American Control Conference*, 2016, pp. 2092–2097.

[8] D. P. Kelly and R. S. Sharp, "Time-optimal control of the race car: a numerical method to emulate the ideal driver," *Vehicle System Dynamics*, vol. 48, no. 12, pp. 1461–1474, 2010.

[9] J. P. Timings and D. J. Cole, "Minimum manoeuvre time of a nonlinear vehicle at constant forward speed using convex optimisation," in *International Symposium on Advanced Vehicle Control*, 2010.

[10] R. Verschueren, S. De Bruyne, M. Zanon, J. V. Frasch, and M. Diehl, "Towards time-optimal race car driving using nonlinear mpc in real-time," in *IEEE Conference on Decision and Control*, 2014, pp. 2505–2510.

[11] R. Verschueren, M. Zanon, R. Quirynen, and M. Diehl, "Time-optimal race car driving using an online exact hessian based nonlinear mpc algorithm," in *European Control Conference*, 2016, pp. 141–147.

[12] L. Van den Broeck, M. Diehl, and J. Swevers, "A model predictive control approach for time optimal point-to-point motion control," *Mechatronics*, vol. 21, no. 7, pp. 1203–1212, 2011.

[13] ——, "Model predictive control for time-optimal point-to-point motion control," in *IFAC World Congress*, 2011, pp. 2458–2463.

[14] R. L. Sutherland, I. V. Kolmanovsky, A. R. Girard, F. A. Leve, and C. D. Petersen, "On closed-loop lyapunov stability with minimum-time mpc feedback laws for discrete-time systems," in *IEEE Conference on Decision and Control (CDC)*, 2019, pp. 5231–5237.

[15] D. Lam, "A model predictive approach to optimal path-following and contouring control," PhD Thesis, The University of Melbourne, 2012.

[16] T. Besselmann, J. Lofberg, and M. Morari, "Constrained time-optimal control of linear parameter-varying systems," in *Joint IEEE Conference on Decision and Control and Chinese Control Conference*, 2009, pp. 6923–6928.

[17] S. Al Homsi, "Online generation of time-optimal trajectories for industrial robots in dynamic environments," PhD thesis, Université Grenoble Alpes, 2016.

[18] C. Rösmann, F. Hoffmann, and T. Bertram, "Timed-elastic-bands for time-optimal point-to-point nonlinear model predictive control," in *European Control Conference*, 2015, pp. 3357–3362.

[19] C. Rösmann, A. Makarow, F. Hoffmann, and T. Bertram, "Sparse shooting at adaptive temporal resolution for time-optimal model predictive control," in *IEEE Conference on Decision and Control*, 2017, pp. 5551–5556.

[20] C. Rösmann, "Time-optimal nonlinear model predictive control – Direct transcription methods with variable discretization and structural sparsity exploitation," Dissertation, TU Dortmund University, 2019.

[21] D. P. Bertsekas, *Dynamic Programming and Optimal Control*. Athena Scientific, 1995.

[22] F. Blanchini and S. Miani, *Set-Theoretic Methods in Control*, 2nd ed. Birkhäuser Basel, 2015.

[23] S. Horiuchi, "Evaluation of chassis control algorithms using controllability region analysis," in *The Dynamics of Verhicles on Roads and Tracks*, M. Rosenberger, M. Plöchl, K. Six, and J. Edelmann, Eds. CRC Press, Taylor & Francis Group, 2015, pp. 35–44.

[24] T. Kailath, *Linear Systems*. Prentice-Hall, 1980.

[25] J. Nocedal and S. J. Wright, *Numerical Optimization*, 2nd ed., ser. Springer series in operations research. New York: Springer, 2006.

[26] D. Nešić and A. R. Teel, "A framework for stabilization of nonlinear sampled-data systems based on their approximate discrete-time models," *IEEE Transactions on Automatic Control*, vol. 49, no. 7, pp. 1103–1122, 2004.

[27] C. Rösmann, M. Krämer, A. Makarow, F. Hoffmann, and T. Bertram, "Exploiting sparse structures in nonlinear model predictive control with hypergraphs," in *IEEE/ASME International Conference on Advanced Intelligent Mechatronics*, 2018, pp. 1332–1337.

[28] D. Q. Mayne, J. B. Rawlings, C. V. Rao, and P. Scokaert, "Constrained model predictive control: Stability and optimality," *Automatica*, vol. 36, no. 6, pp. 789–814, 2000.

[29] L. Chisci, A. Lombardi, and E. Mosca, "Dual-receding horizon control of constrained discrete time systems," *European Journal of Control*, vol. 2, no. 4, pp. 278–285, 1996.

[30] H. Michalska and D. Q. Mayne, "Robust receding horizon control of constrained nonlinear systems," *IEEE Transactions on Automatic Control*, vol. 38, no. 11, pp. 1623–1633, 1993.

[31] C. C. Chen and L. Shaw, "On receding horizon feedback control," *Automatica*, vol. 18, no. 3, pp. 349–352, 1982.

[32] E. M. James, "Time optimal control and the van der pol oscillator," *IMA Journal of Applied Mathematics*, vol. 13, no. 1, pp. 67–81, 1974.

[33] A. Wächter and L. T. Biegler, "On the implementation of a primal-dual interior point filter line search algorithm for large-scale nonlinear programming," *Mathematical Programming*, vol. 106, no. 1, pp. 25–57, 2006.

[34] Computational Mathematics Group, "HSL. A collection of Fortran codes for large scale scientific computation." [Online]. Available: http://www.hsl.rl.ac.uk/

[35] B. Stellato, G. Banjac, P. Goulart, A. Bemporad, and S. Boyd, "Osqp: an operator splitting solver for quadratic programs," *Mathematical Programming Computation*, 2020.

[36] C. Rösmann, "control_box_rst." [Online]. Available: https://github.com/rst-tu-dortmund/control_box_rst